IEEE Antennas and Propagation Magazine, v. 50, no. 3, June 2008

Radiation Efficiency of Nanoradius Dipole Antennas in the Microwave and Far-Infrared Regime

G.W. Hanson, Senior Member

***Abstract*— At microwave and far-infrared frequencies, the radiation efficiency of a wire antenna with radius values smaller than a few hundred nanometers is very low, due to large wire impedances and associated high ohmic losses. However, with the continued miniaturization of electronic devices, nanoradius interconnects and antennas are desirable. In this work, the relationship between wire radius, conductivity, frequency, and ohmic loss is examined for dipole antennas. Simple formulas are derived for the distributed resistance, effective conductivity, and radius required to achieve a desired radiation efficiency, and particular emphasis is given to half-wavelength antennas. Several methods to improve antenna efficiency at sub-100 nm radius values are discussed, including the use of superconducting nanowires and multi-wall carbon nanotubes.**

***Index Terms*— nanoantenna, nanotechnology, carbon nanotube**

I. Introduction

The radiation efficiency (power radiated divided by power input) of a typical half-wavelength dipole antenna is excellent, usually above 98% for frequencies in the microwave regime [1]. This assumes that the antenna is constructed using high-conductivity metals, and that wire radius values are in the typical range, usually from tens of microns through perhaps tens of millimeters, or even larger, depending on frequency. However, there is currently a lot of interest in developing nanoscopic circuits, and nanoscopic autonomous devices for medical or military applications. An important consideration is establishing a wireless communication link, and/or wireless power transfer, to such devices [2]. Obviously, for interfacing with a device having its largest dimension on the order of tens of nanometers, a similarly physically small antenna would be desirable. One possibility may be afforded by the optical range, where sub-wavelength focusing is possible due to plasmonic effects [3]–[10], although atmospheric propagation at optical frequencies is not feasible for long-range communications. Lower frequencies (far-infrared and below) provide more desirable propagation characteristics. However, in the range 1 GHz–1 THz, wavelength varies from 10^8 to 10^5 nanometers, and an electrically very short, extremely thin wire nanoscale dipole has an exceeding small radiation efficiency. For example, at 1 GHz a 200 nm long, 50 nm radius copper wire dipole antenna has radiation efficiency $\varepsilon_{rad} \sim 10^{-8}$ %, and $\varepsilon_{rad} \sim 10^{-2}$ % at 1 THz.

Alternatively, depending on the available real estate on the device or surrounding support structure, it may be feasible to fabricate a half-wavelength or similar antenna that would be very long with respect to nanometers, but which has a radius in the nanometer range. Such an antenna would be invisible to the eye, and could still be connected to the nanodevice because of its small radius. Therefore, the purpose of this work is 1) to illustrate the problems associated with nanoscale radius wires at far-infrared frequencies and below, and 2) to consider what may be able to be accomplished from the material side to improve radiation efficiencies for nanoscale radius wires. The first part is accomplished by considering the surface-impedance integral equation for a lossy antenna, and the connection between the current on an antenna and that associated with the discrete mode excited by a source on an infinite material cylinder. The second part leads to consideration of superconducting nanowires, multi-wall carbon nanotubes, and carbon nanotube bundles.

Department of Electrical Engineering, University of Wisconsin-Milwaukee, 3200 N. Cramer St., Milwaukee, Wisconsin 53211.

II. Modal Interpretation of Antenna Current

Fig. 1 shows the radiation efficiency for a half-wavelength copper dipole at $f = 10$ GHz, 100 GHz, and 1 THz as a function of wire radius, obtained from the surface-impedance integral equation (IE) described below. It can be seen that efficiency is close to unity at all frequencies for radius values greater than several thousand nanometers, but falls precipitously as radius is diminished.

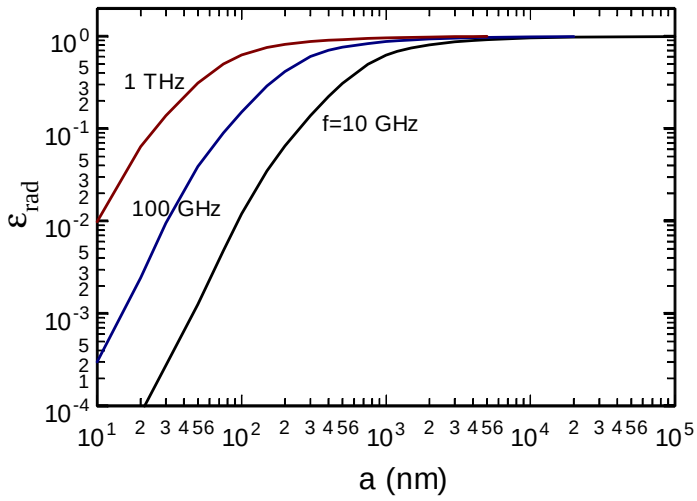

Fig. 1. Radiation efficiency (not percentage) for a half-wavelength copper dipole at $f = 10$ GHz, 100 GHz, and 1 THz as a function of wire radius. Results were computed assuming the bulk value of conductivity.

In order to understand this effect, consider an electrically-thin wire antenna with axis coincident with the z-axis, having radius a and conductivity σ, and residing in free space. The standard integral equation for the antenna current is associated with the impedance boundary condition [11]–[13]

$$I^a(z)\, z_s = E_s(z) \tag{1}$$

at $\rho = a$, where $I^a(z)$ is the antenna current, z_s is the surface impedance (Ω/m), and E_s is the total tangential electric field. The surface impedance is given as [14]

$$z_s = \frac{\gamma J_0(\gamma a)}{2\pi a \sigma J_1(\gamma a)}, \tag{2}$$

where

$$\gamma = (1-j)\sqrt{\frac{\omega\mu_0\sigma}{2}}, \tag{3}$$

and σ is the conductivity of the metal (S/m).

Expressing the electric field as the sum of an impressed field, E_z^i, and the field due to the resulting current leads to the standard Pocklington equation for the thin wire antenna in free-space [11], [15]. Transforming the Pocklington equation to the Hallén form [1], [16]–[17] results in

$$\begin{aligned}\int_{-L}^{L} &\left(K(z-z') + q(z-z')\right) I^a(z')dz' \\ &= c_1 \sin k_0 z + c_2 \cos k_0 z \\ &\quad - \frac{j4\pi}{\eta}\int_0^z E^i(z')\sin\left(k_0(z-z')\right)dz'\end{aligned} \tag{4}$$

for $-L \le z \le L$, where $2L$ is the wire length, $c_{1,2}$ are unknown constants, $\eta = \sqrt{\mu_0/\varepsilon_0}$, $k_0 = \omega\sqrt{\mu_0\varepsilon_0}$,

$$K(z-z') = \frac{1}{2\pi}\int_{-\pi}^{\pi} \frac{e^{-jk_0\sqrt{(z-z')^2+4a^2\sin^2(\phi'/2)}}}{\sqrt{(z-z')^2+4a^2\sin^2\left(\phi'/2\right)}}d\phi', \tag{5}$$

and

$$q(z-z') = 2\pi\omega\varepsilon_0 z_s \frac{e^{-jk_0|z-z'|}}{k_0}. \tag{6}$$

In this work a rectangular pulse function expansion, point testing solution of (4) was obtained, where matrix entries were computed with the aide of the integrals given in [18].

The behavior of nano-radius wire antennas differs from macro-radius wire antennas principally because the exceedingly small radius results in a large surface impedance from (2), which leads to strong current damping and low radiation efficiency. A complementary viewpoint that is illustrative for antenna as well as interconnect applications is obtained by considering the modal (discrete and continuous) representation of current on a driven infinite-length wire, in which case the strong current damping is due to the strong attenuation of the principle discrete propagation mode. This view can be fruitfully examined by considering the spectral characteristics of an infinite dielectric cylinder having radius a and complex permittivity ε_m, where conductivity and permittivity are related by $\sigma = j\omega\varepsilon_0(\varepsilon_m/\varepsilon_0 - 1)$ for a good metal. In this case the current induced by a magnetic frill source of radius b is [13], [19],

$$I(z) = j\omega\varepsilon_m\varepsilon_0 b\int_{-\infty}^{\infty}\frac{J_1(\kappa_m a)H_1^{(2)}(\kappa_0 b)}{Z^e(\gamma)}e^{-j\gamma z}d\gamma, \tag{7}$$

where

$$Z^e(\gamma) = \varepsilon_m\kappa_0 J_1(\kappa_m a)H_0^{(2)}(\kappa_0 a) - \varepsilon_0\kappa_m J_0(\kappa_m a)H_1^{(2)}(\kappa_0 a) \tag{8}$$

with $\kappa_m^2 = k_m^2 - \gamma^2$, $\kappa_0^2 = k_0^2 - \gamma^2$, and $k_m^2 = \omega^2\mu_0\varepsilon_m$. The zeros of $Z^e(\gamma)$ represent the symmetric TM modes of the dielectric cylinder. Following the method detailed in [16, pp. 451–453] (see also [19, pp. 377-380]), the integral (7) can be written as a branch cut integral (continuous spectrum) and a sum of residues (discrete spectrum) [13],

$$I(z) = \sum_n I_n(z) + I_{bc}(z). \tag{9}$$

Of course, the modes diffract at the ends of a finite-length cylinder, and this diffraction is difficult to model exactly. However, as discussed in [14], for a metallic wire only the principle mode ($n = 0$) is not highly attenuated, and so the usual standing wave current on a resonant half-wavelength dipole antenna can be viewed as due to constructive interference between the principle mode travelling outwards from the source and its (approximately open-circuit) reflection from the wire ends. In the following, the principle mode will be denoted as $\beta = \gamma_{n=0}$.

To verify that the current on a wire antenna is indeed the aforementioned modal current, Fig. 2 shows the magnitude of the current induced by a magnetic frill source on a copper wire having $a = 1$ μm at $f = 10$ GHz (current is symmetric, and so only $I(z)$ for $z \ge 0$ is shown). The solid curve is obtained from (9) for the infinite wire, and includes both the principle mode residue and the branch cut contribution (details of the calculation can be found in [13]). The solid squares are obtained from the IE (4), where $L = 40\lambda$ so that current has decayed sufficiently upon reaching the wire ends to insure that no reflection occurs (allowing comparison with the infinite wire case). Agreement between the two methods is excellent. Also shown is the residue contribution alone (dashed curve), where, as would be expected, the discrete principle mode dominates the response except in the vicinity of the source.

It should be noted that the modal form (9) is an exact solution for an infinite-length wire, and merely requires evaluating a residue and an integration, whereas the IE (4) is itself an approximate relationship, based on an impedance boundary condition, and requires a further approximation in obtaining the solution via discretization. Therefore, the good agreement between the modal method and the IE solution gives confidence in the surface impedance IE for the considered structure.

The low radiation efficiency of a half-wavelength nano-radius antenna can be understood from the large surface impedance (2), or from the propagation characteristics of the principle mode on an infinite length wire. Fig. 3 shows the real and imaginary parts of the principle mode β as a function of wire radius for a copper wire. For sufficiently large radius, $\mathrm{Re}(\beta) \simeq k_0$ and $\mathrm{Im}(\beta) \ll \mathrm{Re}(\beta)$, as expected, and therefore current resonances on a finite-length dipole antenna occur when $2L \simeq n\lambda/2$, $n = 1, 2, ...$, where λ is the free-space wavelength. Since phase velocity is $v_p = \omega/\mathrm{Re}(\beta)$, for nano-radius values the principle mode becomes very slow, and highly attenuated. Note also that since the values are normalized by k_0, the attenuation at 100 GHz is actually more severe that at 10 GHz, even though the 100 GHz curve is below

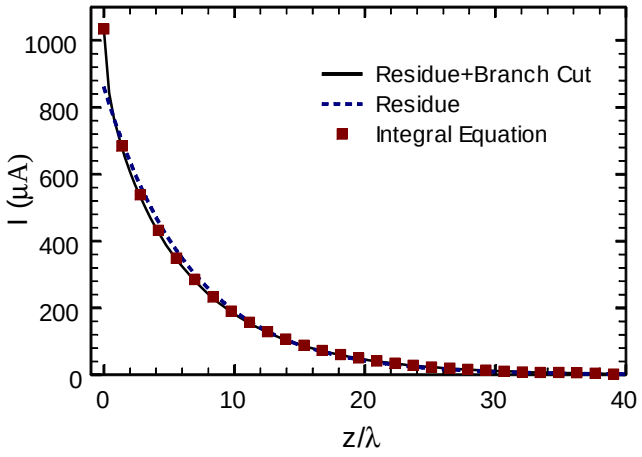

Fig. 2. Magnitude of the current induced by a magnetic frill source ($b = 1.2a$) on a copper wire having $a = 1$ μm at $f = 10$ GHz. The solid curve is obtained from the exact modal method (9) for the infinite wire, and includes both the principle mode residue and the branch cut contribution. The solid squares are obtained from the IE (4), where $L = 40\lambda$ to model an infinite length wire. The dashed curve is the principle residue term.

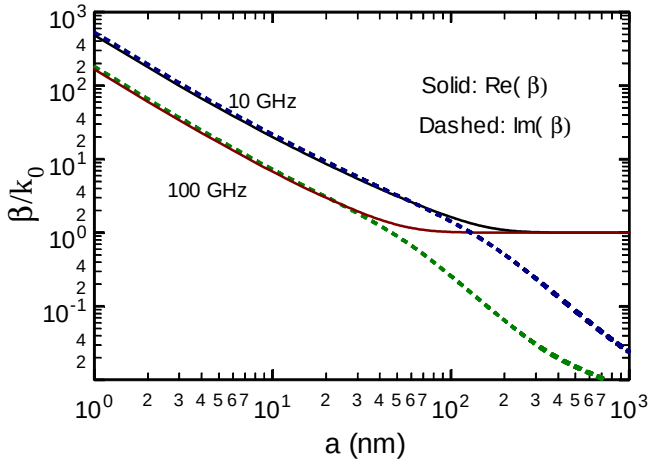

Fig. 3. Real and imaginary parts of the principle discrete mode β as a function of wire radius for a copper wire.

the 10 GHz curve on the plot.

III. Metal Conductivity and Surface Impedance at the Nanoscale

Before discussing further results, a discussion of metal conductivity at the nanoscale is warranted. The conductivity of bulk metal in the far-infrared and microwave regimes (i.e., ignoring interband electronic transitions) is given by the Drude form [20]

$$\sigma_b(\omega) = \frac{e^2 N_e \tau}{m_e(1 + j\omega\tau)} = \frac{\sigma_0}{1 + j\omega\tau}, \tag{10}$$

where σ_0 is the dc conductivity, N_e is the three-dimensional electron density, m_e is the electron mass, $-e$ is the charge of an electron, and τ is the electronic relaxation time. For copper, $N_e \simeq 8.46 \times 10^{28}$ electrons/m^3 and $\tau \simeq 2.47 \times 10^{-14}$ s [20], leading to $\sigma_0^{Cu} = 5.9 \times 10^7$ S/m. For bulk gold, $\sigma_0^{Au} \simeq 4.6 \times 10^7$ (S/m).

For ordinary conductors having dimensions on the order of the electronic mean free path (L_m) or less, the dc conductivity value σ_0 is changed from the bulk value. For copper, the mean free path is approximately 40 nm at room temperature, and for wires having effective radius values in this range, size-dependent (mean-free path, not quantum confinement) effects are important. This is due to scattering from the metal's surface, and from grain boundaries [21]–[22]. A simple approximate formula for the radius-dependent dc conductivity of a circular cross-section wire is [22]

$$\sigma_0(a) = r(a)\,\sigma_0, \tag{11}$$

$$r(a) = \left(1 + (1-p)\frac{L_m}{2a}\right)^{-1}, \tag{12}$$

where p is the specularity parameter for electron reflection from the wire surface. This model was applied in [22] to copper and silver wires with radius values a as small as 7 nm, and good agreement with measurement was found. The model (11) ignores grain-boundary scattering, which can further reduce conductivity, although grain-boundary scattering can be avoided; for example, in [22] transmission electron microscopy (TEM) showed that their samples had no significant grain boundaries. A model for rectangular cross-section wires that also includes grain-boundary scattering is provided in [21], with the result that the form (11) is still valid with a modified function $r(a)$.

For the results in Fig. 3 and in all subsequent figures, (11) was used with $p = 0.5$ [22], which, since grain-boundary scattering is ignored, represents a best-case scenario. The efficiencies in Fig. 1 were computed using the bulk conductivity, and so the small-radius values would be even worse if (11) was included. Note that the use of the radius-dependent conductivity (11) has only so-far been verified for dc – at this point it has not been experimentally confirmed that (11) needs to be used in (10) for GHz-THz frequencies. However, given the fact that $\omega\tau \ll 1$ in this frequency range, it is likely that (11) applies at least through the lower THz range.

The surface impedance (2) has a resistive part, accounting for dissipation, and a reactive part, accounting for inductance. Because we are interested in very small radius wires, and because of the importance of kinetic inductance in this limit, and for carbon nanotubes discussed later, it is worthwhile to consider z_s in the small radius limit. Upon expanding the Bessel functions as $J_0(\gamma a) \simeq 1 - (\gamma a)^2/4$ and $J_1(\gamma a) \simeq (\gamma a)/2 - (\gamma a)^3/16$ for $|\gamma a| \ll 1$ [23] (i.e., when radius is much smaller than the shin depth), using the binomial expansion in the dominator and keeping terms up to quadratic order, then

$$z_s = R_{sr} + j\omega(L_k + L_s), \tag{13}$$

for $|\gamma a| \ll 1$, where, writing $\sigma = \sigma_r - j\sigma_i$,

$$R_{sr} = \frac{\sigma_r}{\pi a^2 \left(\sigma_r^2 + \sigma_i^2\right)}, \quad L_k = \frac{\sigma_i}{\pi a^2 \omega \left(\sigma_r^2 + \sigma_i^2\right)}, \quad L_s = \frac{\mu_0}{8\pi}. \tag{14}$$

L_k is the kinetic inductance (H/m) due to energy associated with the inertial mass of the electrons [24], and L_s is the usual self (internal) inductance (H/m) of a long straight nonmagnetic wire [14]. Both inductance expressions can be derived by independent methods by assuming that current is uniformly distributed over the cross-section of the wire.

For lower THz frequencies and below, where $\omega\tau \ll 1$ such that $\sigma \simeq \sigma_0(a)(1 - j\omega\tau)$,

$$R_{sr} \simeq \frac{1}{\pi a^2 \sigma_0(a)} = \frac{m_e}{\pi a^2 e^2 N_e \tau} \frac{1}{r(a)}, \quad L_k = \tau R_{sr}. \tag{15}$$

For macroscopic radius wires $L_k \ll L_s$, and so typically kinetic inductance is ignored compared to other inductances in the system. However, for extremely small radius wires R_{sr} is very large, and the kinetic inductance τR_{sr} can be much larger than L_s. From (15) and ignoring the $r(a)$ factor, it is easy to see that for $a \leq \sqrt{8m_e/\mu_0 e^2 N_e}$ kinetic inductance will be larger than self-inductance. For copper $a \leq 51$ nm, which increases to 56 nm when $r(a)$ is included. Furthermore, excepting superconductors, the kinetic reactance $\omega\tau R_{sr}$ will be small compared to the ohmic resistance R_{sr}. For copper, $\omega\tau = 1$ when $f = 6.44$ THz, and so well below this frequency ohmic resistance is the dominate contribution to the surface impedance.

Note that from (10), the effect of reduced conductivity (11) due to mean-free-path effects corresponds to an effective reduction in the carrier density. Therefore, this effect can be incorporated in the kinetic inductance and ohmic resistance terms (15) by replacing σ_0 with $\sigma_0(a) = r(a)\sigma_0$, or by replacing N_e with $r(a)N_e$. The described radius-dependent effect on conductivity is expected to be valid down to radius values of a few nanometers. Below this, because the Fermi wavelength of electrons in typical metals is approximately 0.5 nm, quantum confinement effects become important.

Using the standard formula for power attenuation,

$$A_p = 8.686 \ \mathrm{Im}(\beta) \ \text{dB/m}, \tag{16}$$

Fig. 4 shows the attenuation (dB/μm) for the principle mode at $f = 100$ GHz (similar results corresponding to the $f = 10$ GHz data in Fig. 3 are omitted for clarity). The lower solid curve was computed assuming bulk copper conductivity, the upper solid curve assumes bulk gold conductivity, and the dashed curves are the corresponding results using the reduced conductivity (11). Also shown is the conductivity profile $\sigma_0(a)/\sigma_0 = r(a)$ from (11)–(12). It can be seen that attenuation dramatically increases as wire radius decreases, and that for radius values less than a few hundred nanometers, conductivity reduction due to radius dependent effects, and the associated increase in attenuation, are important.

IV. Requirements for Obtaining a Desired Radiation Efficiency

In order to achieve good radiation efficiency using a nanoscale radius wire, it is necessary to maintain a sufficiently small wire impedance per unit length. From

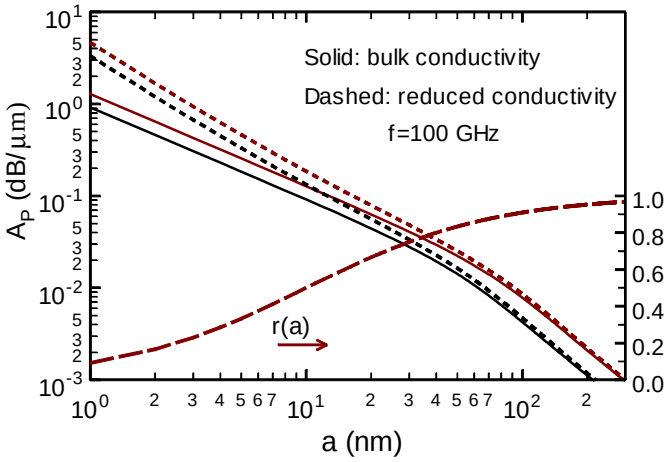

Fig. 4. Attenuation (dB/μm) for the principle discrete mode at $f = 100$ GHz. Lower solid curve: bulk copper, upper solid curve: bulk gold, dashed curves are the corresponding results using the reduced conductivity (11). Also shown is the radius-dependent conductivity profile (right axis) from (12).

$$\varepsilon_{rad} = \frac{R_{rad}}{R_{rad} + R_{ohmic}}, \tag{17}$$

where R_{rad} is the radiation resistance and R_{ohmic} is the ohmic resistance, the required ohmic resistance to achieve a desired radiation efficiency is

$$R_{ohmic}^{req} = R_{rad}\left(\frac{1}{\varepsilon_{rad}} - 1\right). \tag{18}$$

The ohmic resistance associated with a given current distribution on an antenna can be written as the product of a per-unit-length resistance R' that only depends on the wire material, and a length parameter L_0 that depends on the current profile along the antenna [1],

$$R_{ohmic} = R' L_0, \tag{19}$$

where

$$R' = \mathrm{Re}(z_s) \tag{20}$$

(Ω/m). This comes from the definition of $R_{ohmic} = 2P_{ohmic}/|I_{in}|^2$, with

$$P_{ohmic} = \mathrm{Re}(z_s) \int \frac{1}{2} |I(z)|^2 \, dz, \tag{21}$$

and therefore

$$L_0 = \frac{1}{|I_{in}|^2} \int |I(z)|^2 \, dz \tag{22}$$

where the integration is taken over the length of the antenna (in this case the current is taken as filamentary, and any skin-depth effects are accounted for via z_s). From (18) and (19), the required per-unit-length resistance to achieve a desired radiation efficiency is therefore

$$R'_{req} = \frac{R_{rad}}{L_0}\left(\frac{1}{\varepsilon_{rad}} - 1\right). \tag{23}$$

As an example, for a half-wavelength dipole assuming a sinusoidal current distribution, $L_0 = \lambda/4$. For a triangular current on a dipole of length $2L \ll \lambda$, (electrically short dipole, ESD), $L_0 = 2L/3$, and for a constant current on an antenna of length $2L$, $L_0 = 2L$ [1]. The radiation resistance for a half-wavelength dipole is approximately $R_{rad}^{\lambda/2} \simeq 73$ ohms, so that the required value of R' is

$$R'_{req}\big|_{\lambda/2} = \frac{4\,(73)}{\lambda}\left(\frac{1}{\varepsilon_{rad}} - 1\right), \tag{24}$$

which is shown in Fig. 5 for three frequencies of interest.

Regarding the accuracy of the formulas, note that the radiation resistance value of 73 ohms assumes an ideal sinusoidal current. For high ohmic losses the current changes from sinusoidal to damped, and $R_{rad}^{\lambda/2} = 73$ ohms is no longer valid. This occurs approximately when $\varepsilon_{rad} < 10\%$, and so (24) is only valid for $\varepsilon_{rad} \gtrsim 0.1$. (23) is more general, but the formula is really only practically useful when L_0 and R_{rad} can be reasonably approximated by their values from simple theory.

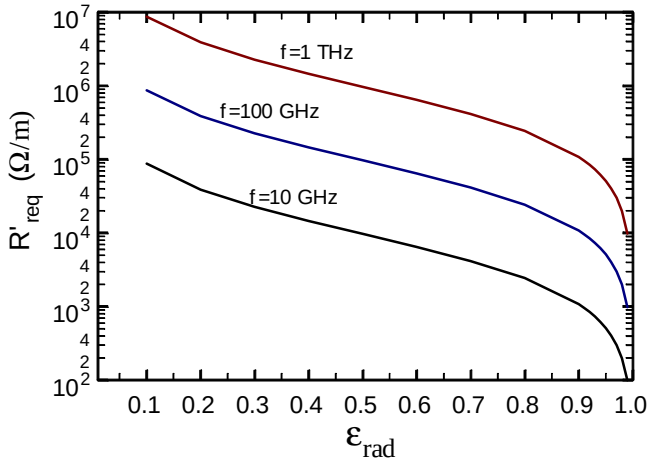

Fig. 5. Required distributed resistance to achieve a given value of ε_{rad} at $f = 10$, 100, and 1000 GHz for a half-wavelength dipole.

For a short dipole [1]

$$R_{rad}^{ESD} = 20\pi^2\left(\frac{2L}{\lambda}\right)^2, \tag{25}$$

and so the required distributed resistance is

$$R'_{req}\big|_{ESD} = \frac{120\pi^2 L}{\lambda^2}\left(\frac{1}{\varepsilon_{rad}} - 1\right), \tag{26}$$

which is valid assuming a triangular current distribution. For example, assuming a desired radiation efficiency of 50% at $f = 10$ GHz, $R'_{req}\big|_{\lambda/2} \simeq 9.7 \times 10^3$ Ω/m, and $R'_{req}\big|_{ESD} \simeq 395$ Ω/m for an $L = \lambda/100 = 300$ μm dipole.

An explicit expression can be determined for the required metal conductivity to achieve a given value of radiation efficiency, for the case of wire radius much less than the skin depth and $\omega\tau \ll 1$ in (10). Equating R_{sr} in (15) to the right-side of (23) leads to

$$\sigma_{req}\,(a) \simeq \left[\frac{\pi a^2 R_{rad}}{L_0}\left(\frac{1}{\varepsilon_{rad}} - 1\right)\right]^{-1}. \tag{27}$$

The resulting value of conductivity agrees very well with numerical tests using the integral equation (4). For wire radius not necessary small compared to skin depth, the desired value of σ_{req} can be found from

$$\mathrm{Re}\,(z_s) - \frac{R_{rad}}{L_0}\left(\frac{1}{\varepsilon_{rad}} - 1\right) = 0. \tag{28}$$

Fig. 6 shows the value of σ_{req} (normalized by the bulk dc copper value, σ_0) to achieve the indicated radiation efficiency for a half-wavelength dipole antenna as a function of radius at $f = 10$ GHz. The required values for an electrically short antenna are much larger, and won't be discussed here. The conductivity of copper from (11) is also shown (normalized by σ_0, and ignoring grain-boundary scattering, leading to a best-case result). It can be seen that, for example, if $\varepsilon_{rad} = 1\%$ is tolerable, wire radius of a copper dipole can be as small as 100 nm (since the current is strongly perturbed from a sinusoid for $\varepsilon_{rad} = 1\%$, (4) rather than (27) was used to compute this curve - for the other two efficiencies shown (4) and (27) give approximately the same result). If $\varepsilon_{rad} = 10\%$ is required, the radius of a copper dipole must be 250 nm. Although not shown on the scale of the graph, if $\varepsilon_{rad} = 50\%$ is required, for a copper dipole the radius must be 750 nm. The curve labeled MWCNT will be discussed later.

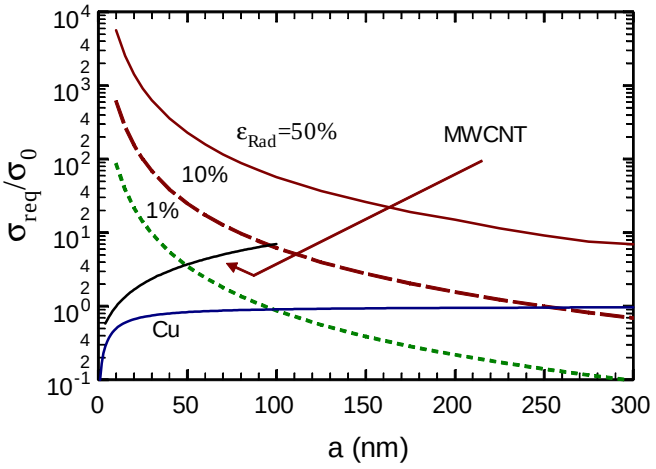

Fig. 6. Required conductivity σ_{req} to achieve the indicated radiation efficiency for a half-wave dipole antenna as a function of radius at $f = 10$ GHz. The curve labeled MWCNT will be discussed later, and the curve labeled Cu is $r\,(a)$ given by (11). $\sigma_0 = 5.9 \times 10^7$ S/m is the bulk dc conductivity of copper.

Fig. 7 shows the required conductivity to maintain 50% radiation efficiency for a half-wavelength dipole antenna at several different frequencies. As frequency increases, good radiation efficiency can be maintained for fairly small radius

values (e.g., $\varepsilon_{rad} = 50\%$ for a copper dipole having $a = 80$ nm at 1 THz). This trend of decreasing minimum radius with increasing frequency extends into the far-infrared, but for frequencies such that $\omega\tau > 1$, conductivity begins to drop from (10). Note that at 1 THz, $\lambda/2 = 150$ μm, and so an antenna having $a = 80$ nm and $2L = 150$ μm is physically quite small, although the length of the antenna is very long compared to nanometers. Since the conductivity of gold is similar to copper in the examined frequency range, results for gold wires will be very similar to those for copper, and are omitted.

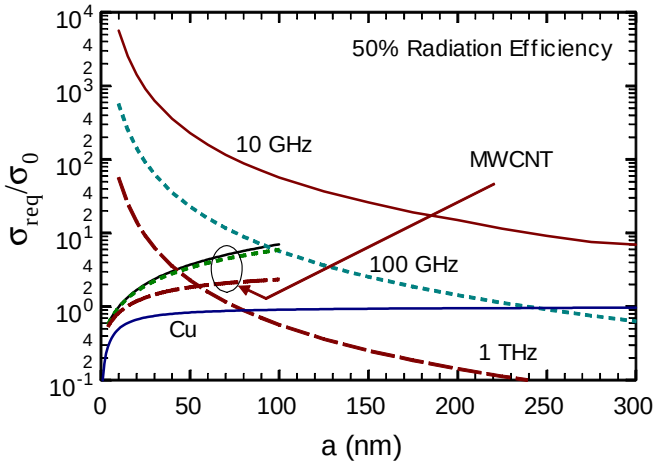

Fig. 7. Required conductivity to maintain 50% radiation efficiency for a half-wave dipole antenna at several different frequencies. The curves labled MWCNT will be discussed later, and the curve labeled Cu is $r\,(a)$ given by (11). $\sigma_0 = 5.9 \times 10^7$ S/m is the bulk dc conductivity of copper.

Finally, if grain-boundary scattering can be ignored, equating (27) and (12) leads to the required wire radius to achieve a certain radiation efficiency, a_{req}, given for $\omega\tau \ll 1$ by the solution of

$$a_{req}^3 \left(\frac{\pi\sigma_0 R_{rad}}{L_0} \left(\frac{1}{\varepsilon_{rad}} - 1 \right) \right) - a_{req} - (1-p)\,\frac{L_m}{2} = 0, \tag{29}$$

where σ_0 is the bulk dc conductivity. If the value of a_{req} is at least a few times the term $(1-p)\,L_m/2$ ($\simeq 10$ nm for copper with $p = 0.5$), then

$$a_{req} \simeq \sqrt{\left(\frac{\pi\sigma_0 R_{rad}}{L_0} \left(\frac{1}{\varepsilon_{rad}} - 1 \right) \right)^{-1}}. \tag{30}$$

From the preceding figures, the question arises as to what can be done to achieve the required conductivity values if, for a given combination of frequency and radius, the resulting efficiency using an ordinary metal is not adequate. Several possible solutions are discussed next.

V. Low Temperatures and/or Superconducting Materials

One method to increase bulk conductivity is to lower the temperature, while still using ordinary (not superconducting) materials. The conductivity of copper (gold and other high-conductivity metals are qualitatively similar) as a function of temperature is shown in Fig. 8, where σ_0 is the dc, room temperature value of bulk conductivity. It can be seen that for bulk copper at liquid nitrogen temperatures ($\simeq 77$ K) conductivity is an order of magnitude larger than at room temperature, while at liquid helium temperatures ($\simeq 4$ K), conductivity is increased by three orders of magnitude compared to room temperature.

Unfortunately, this increased conductivity cannot be used to achieve high radiation efficiencies in nanoradius wire antennas because of radius-dependent effects. Referring to (12), the term L_m/σ_0 is independent of temperature [22], whereas the bulk conductivity σ_0 increases with temperature. Since the radius-dependent term in (11) is constant with respect to temperature, the nano-radius wire conductivity does not increase substantiality as temperature is lowered, even as $T \to 0$ K. This is shown in Fig. 8 for various radius values, where the data for bulk copper is from [25]. Hence, using ordinary conductors and lowering the temperature is not a feasible option to increase nanoradius wire conductivity.

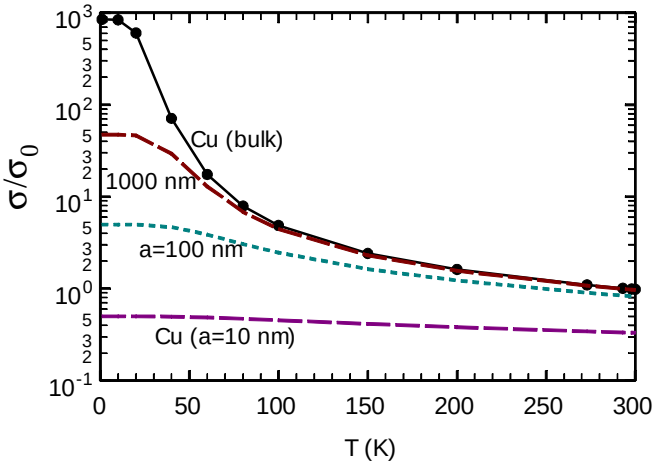

Fig. 8. Conductivity of copper as a function of temperature, where σ_0 is the dc, room temperature value of bulk conductivity. The result for bulk copper is shown (data from [25]), as well as for wires with various radius values.

Although radius-dependent effects limit low-temperature ordinary conductivity, the use of superconducting nanowires is possible. Superconductivity is a macroscopically coherent electronic state, and a basic question is the effect of nanoscale radius on superconducting wire properties. However, it has been shown that superconductivity exists in nanowires with radius values as small as $a = 6$ nm [26]–[28], opening up the possibility of superconducting nanowire interconnects and antennas. A complete survey on the use of superconductors in antenna applications is beyond the scope of this work, and here we simply note the summaries in [29] and [30]. As a concrete example, niobium has been considered for superconducting nanoscale radius interconnects [31]–[32] due to its good mechanical stability and electrical properties. The

complex conductivity can be written as [24], [32]

$$\sigma_{sc}(\omega,T)=\sigma_r(\omega,T)-j\sigma_i(\omega), \tag{31}$$

where

$$\sigma_r=\sigma_n\frac{2\Delta}{k_BT}\frac{e^{\frac{\Delta}{k_BT}}}{\left(1+e^{\frac{\Delta}{k_BT}}\right)^2}\ln\left(\frac{\pi\Delta}{e\Phi_0\omega}\right), \tag{32}$$

$$\sigma_i(\omega)=\frac{1}{\omega\mu_0\lambda_L^2}, \tag{33}$$

where $\sigma_n=27.8$ MS/m is the normal conductivity of niobium just above the critical temperature $T_C\simeq 9.3$ K, k_B is Boltzmann's constant, $2\Delta=3.05$ meV is the gap energy, $\Phi_0=h/2e$ is the flux quantum (h is Planck's constant), and $\lambda_L\simeq 86$ nm is the London penetration depth. The expression (32)–(33) is valid in the superconducting state below the gap frequency $f_\Delta=\Delta/e\Phi_0\simeq 738$ GHz.

From (14) and (23), the required radius to achieve a certain radiation efficiency using a superconducting wire is

$$a_{req}^{sc}=\left(\frac{\pi R_{rad}\left(\sigma_r^2+\sigma_i^2\right)}{L_0\sigma_r}\left(\frac{1}{\varepsilon_{rad}}-1\right)\right)^{-1/2}. \tag{34}$$

For niobium at $f=10$ GHz and $T=4.2$ K, Table 1 shows the required radius to achieve the indicated radiation efficiency for a half-wavelength dipole. As a check on (34), good agreement was found with the computed values of ε_{rad} from IE (4) using (31).

ε_{Rad} (%)	a_{req}^{sc} (nm)
75	20
80	23
85	28
90	35
95	51
98	81

Table 1. Required radius a_{req}^{sc} of a niobium half-wavelength dipole antenna at 10 GHz and 4.2 K to produce the indicated radiation efficiency.

Furthermore, since $\sigma_i\gg\sigma_r$ (e.g., at $f=10$ GHz and $T=4.2$ K, $\sigma_{sc}=0.012-j1.7$ GS/m), the expressions (14) reduce to

$$R_{sr}=\frac{\sigma_r}{\pi a^2\left(\sigma_r^2+\sigma_i^2\right)}\simeq\frac{\sigma_r}{\pi a^2\sigma_i^2}, \tag{35}$$

$$L_k\simeq\frac{1}{\pi a^2\omega\sigma_i}. \tag{36}$$

Rewriting

$$R_{sr}=\frac{1}{\pi a^2\frac{\sigma_r^2+\sigma_i^2}{\sigma_r}}=\frac{1}{\pi a^2\sigma_{eff}}, \tag{37}$$

where $\sigma_{eff}\simeq\sigma_i^2/\sigma_r$, then (27) is also valid for superconductors upon replacing $\sigma_0(a)$ with σ_{eff}.

From Table I, it is obvious that very good efficiencies can be achieved using extremely small radius superconducting nanowires. Superconducting nanowires can also obviously be used to improved the efficiency of electrically short dipoles, where the required distributed resistance is given by (26), although superconductivity does not eliminate the small bandwidth problems associated with short antennas [29]. One positive aspect of superconducting antennas is that cooling to cryogenic temperatures may be consistent with the functioning of some nanoelectronic circuits, where suppression of thermal energy is often important in preserving quantum effects.

VI. Carbon Nanotubes

Another possibility for achieving large conductivities is through the use of carbon nanotubes (CNs). Single-wall carbon nanotubes (SWCNTs) are hollow tubes with the tube wall being a mono-atomic layer of hexagonally-bonded carbon atoms [33]. SWCNTs typically have radius values from less than a nanometer to several nanometers, and lengths can be (at least) centimeters. Electrically, carbon nanotubes can be either metallic or semiconducting, depending on their geometry [33].

Carbon nanotubes may be good candidates for nano-antennas and nano-interconnects since they are stronger than conventional metals, and have excellent thermal and electrical properties [33]. SWCNTs can support current densities up to at least 10^9A/cm^2, significantly larger than traditional metals in this size range (typically having maximum current densities on the order of 10^5A/cm^2). The impressive characteristics of CNs are partly due to intrinsic material properties associated with the carbon-carbon bond, but also due to the fact the carbon nanotubes can be fabricated as one-dimensional conductors with very few defects. In comparison, typical nanowires suffer from surface and grain-boundary scattering, electromigration [34], and oxidation (for some materials, such as copper [35]).

Previous work on carbon nanotube antennas considered single wall tubes [2], [17], [36]–[38]. As described below, the very large surface impedance of a SWCNT leads to exceedingly low radiation efficiencies, although the use of carbon nanotube bundles or large-radius multi-wall carbon nanotubes may overcome this problem.

A. Single Wall Carbon Nanotubes

For a SWCNT, the two-dimensional surface conductivity (S) can be obtained from a semiclassical Boltzmann transport equation [39]–[40], leading to

$$\sigma_{cn}(\omega)\simeq\frac{2e^2v_F\tau}{\pi^2\hbar a\left(1+j\omega\tau\right)}=\frac{\sigma_0^{cn}}{\left(1+j\omega\tau\right)}, \tag{38}$$

where v_F is the Fermi velocity ($v_F\simeq 10^6$ m/s), $\hbar$ is the reduced Planck's constant, and τ is the relaxation time which accounts for electron interactions with acoustic phonons [41]. From [42], $\tau=2a/(\alpha T)$, where T is temperature and α is a constant with units m/Ks. The value of α obtained from experiment is in the range $9.2-12$, yielding τ in the range of 10^{-13} to 10^{-12} for typical radius tubes, and here we use $\alpha=12$. For a single-wall carbon nanotube, rather than (2), the distributed impedance

$$z_{cn}=\frac{1}{2\pi a\sigma_{cn}}=R_{cn}+j\omega L_{cn}, \tag{39}$$

(Ω/m) should be used in (4)–(6), where

$$R_{cn} = \frac{h}{4e^2}\frac{1}{2v_F\tau} = \frac{h}{4e^2}\frac{\alpha T}{v_F 4a}, \tag{40}$$

$$L_{cn} = \tau R_{cn} = \frac{1}{4}\frac{h}{2e^2 v_F} \simeq 3.38 \text{ nH}/\mu\text{m}. \tag{41}$$

L_{cn} is the kinetic inductance of the nanotube, in agreement with the value derived by independent methods [43]–[44]. The expression for the ohmic resistance R_{cn} agrees with that obtained in [45].

For a typical tube such as the $(20, 20)$ armchair tube having $a = 1.356$ nm, the room temperature impedance at 10 GHz is $z_{cn} \simeq (4.4 + j0.2)$ kΩ/μm, and $z_{cn} \simeq (6 + j0.2)$ kΩ/μm for $a = 1$ nm. Measurements on good-quality nanotubes having radius values in the $a = 1.5$ nm range has shown a resistance of $R_{cn} \simeq 6$ kΩ/μm at least through 10 GHz [46], in fairly good agreement with (40). Note that since ballistic transport is not contained in (38), the associated impedance, and the presented IE model, is only valid for tubes that are long compared to the mean-free path, which is on the order of a micron for a SWCNT.

A comparison between the conducting qualities of long metallic carbon nanotubes and metals wires is useful. A typical radius of a SWCNT is $1 - 2$ nm, with an impedance of approximately 6 kΩ/μm. For a solid copper wire at 10 GHz, the impedance of a 1 nm radius wire is, from (2) and (11), $z_s \simeq (59 + j0.092)$ kΩ/μm. For a 2 nm wire, $z_s \simeq (8 + j0.013)$ kΩ/μm (the real part is only dependent on radius, and is constant in frequency through the low THz range). These values ignore grain-boundary scattering, which may considerably increase the resistance. Therefore, it can be seen that metallic carbon nanotubes are better conductors than copper wires having similar radius values. However, it is unlikely that good-quality copper wires could be fabricated at these small radius values, and so the comparison is somewhat artificial. In summary, although SWCNTs have an effective conductivity that is greater than a typical metal, a sufficiently large radius metal wire, say, having radius values above $10-20$ nm, will be a much better conductor than a single SWCNT having $a = 1 - 2$ nm.

B. Carbon Nanotube Bundles

The excellent intrinsic properties of SWCNTs lead to promising applications if the large impedance associated with their small radius can be overcome. This naturally leads to the idea of using bundles of CNs to form conducting wires [47]–[50]. As another comparison with copper, consider that a 20 nm radius copper wire with no grain-boundary scattering has an impedance from (2) of 20 Ω/μm through the THz range. Assuming 1 nm radius nanotubes, the same cross-sectional area could accommodate $N = 400$ tubes in a nanotube bundle, and the overall resistance would be (dividing 6 kΩ/μm by N), 15 Ω/μm. As discussed in [49]-[50], dense CN bundles of metallic tubes may have conductivity (per unit cross-sectional area) an order of magnitude greater than metal interconnects, if the radius of the individual nanotubes is sufficiently small. Given the likelihood of significant electron scattering, and of electromigration and other effects in metal nanowires, CN bundles may be an attractive option for nanoradius antennas. However, currently it is more feasible to fabricate large radius multi-wall carbon nanotubes, which also show significant improvements over metals.

C. Multi-Walled Carbon Nanotubes

Multiwall carbon nanotubes (MWCNTs) consist of concentric carbon nanotubes, with the spacing between adjacent walls $\delta \simeq 0.34$ nm, which is the distance between atomic planes in graphite. Viewing each wall of the MWCNT as a SWCNT, each wall should have a distributed resistance (40) (the value of $\alpha \simeq 12$ quoted after (40) is for a SWCNT, resulting in a mean-free path on the order of a micron. For a MWCNT, the mean-free path can on the order $20 - 30$ μm [51], and so the the appropriate value of τ needs to be considered). Thus, N concentric metallic tubes having length on the order of the mean-free path should have a resistance R_0/N, where $R_0 = h/4e^2$, in the same way as an N-tube SWCNT bundle.

However, measured resistance on MWCNTs can be much larger than this value for two principle reasons. First, since some tube walls will generally be semiconducting, assuming those walls don't contribute to conduction reduces the effective value of the number of walls to $M < N$, where M is the number of conducting walls. Second, and most importantly, often electrical contact is only made to the outermost wall, unless special care is taken, in which case the resistance would be approximately R_0.

Fortunately, for relatively large diameter MWCNTs where contact is made to all tube walls, room temperature resistance can be actually be much lower than R_0/N [51]. This can again be attributed to two reasons. First, due to the large diameter, at room temperature any semiconducting tube walls will conduct since the electronic energy gap of a semiconducting nanotube decreases with increasing tube diameter as $E_g \simeq 0.38/d$ eV, where $d = 2a$ is the tube diameter in nanometers. Therefore, for diameters larger than approximately 15 nm the energy gap will be small compared to room temperature thermal energy, which results in, effectively $M \simeq N$. Second, for large wall diameters and sufficiently high temperatures, many electronic subbands can also participate in conduction, lowering the effective value of resistance for each wall (SWCNTs have two electron channels [33]). Measurements in [51] for a 25 μm long MWCNT having $a_{\max} = 50$ nm and $a_{\min} = 25$ nm, where $a_{\max}$ and $a_{\min}$ are the radius values of the outer and inner wall, respectively (thus, approximately 74 walls should be present) show that $R \simeq R_0/230$, rather than $R = R_0/74$ which would be expected using a naive theory. However, it should be appreciated that special care needs to be taken to contact all tube walls.

Based on the work in [51], an expression for MWCNT conductivity (S/m) was developed in [52], and for $D_{\max} > 6$ nm results in

$$\sigma_{mw} = \left[\left(1 - \frac{D_{\max}^2}{D_{\min}^2}\right)\frac{a_0}{2} + \left(b_0 - \frac{L}{l_0}a_0\right) \times \left(\frac{1}{D_{\max}} - \frac{D_{\min}}{D_{\max}^2}\right) - \frac{L}{D_{\max}^2 l_0}\ln\left(\frac{D_{\max} + L/l_0}{D_{\min} + L/l_0}\right)\right]\frac{LG_0}{2\delta}, \tag{42}$$

where $D_{\max\,/\,\min} = 2a_{\max\,/\,\min}$, $l_0 = 1000$, $a_0 = 0.0612$ nm^{-1}, $b_0 = 0.425$, and $G_0 = 2e^2/h$ is the conductance quantum. When the length of the tubes becomes much longer than the mean free path, $L \gg l_0 D_{\max}$, (42) reduces to

$$\sigma_{mw} = \frac{G_0 l_0}{2\delta}\left(\frac{7}{24}a_0 D_{\max} + \frac{3}{8}b_0\right), \tag{43}$$

assuming $D_{\min} = D_{\max}/2$.

The per-unit-length impedance of a hollow conducting tube having conductivity σ_{mw} (S/m) and wall thickness d_{mw} small compared to the skin depth is [11]

$$z_{mw} = \frac{1}{2\pi a\,(\sigma_{mw} d_{mw})}. \tag{44}$$

As a test of (42), in [51] a measured dc resistance of $34.4\,\Omega$ was reported for a MWCNT having $D_{\max} = 100$ nm, $D_{\min} = D_{\max}/2$, and length $L = 25$ μm. Using (44) with (42), $z_{mw}L = 60$ Ω, in reasonable agreement with measurement. As another check, in [53] multi-wall contact was established with a 2.6 μm long, 8.6 nm diameter MWCNT nanotube, and a resistance of 2.4 kΩ was measured. In comparison, (44) predicts 4.5 kΩ. In both cases the developed theory is within a factor of two with experiment.

Assuming the special (but practical) case of $a = a_{\max}$, $d_{mw} = a_{\max} - a_{\min} = a_{\max}/2$, then

$$z_{mw} = \frac{1}{\pi a^2 \sigma_{mw}}, \tag{45}$$

which has the same form as (20). Therefore, σ_{mw} can be directly compared to conductivity for a metal wire. In Fig. 6, the curve labelled MWCNT is σ_{mw}/σ_0, where σ_{mw} is found from (42) for tube length $\lambda/4$ (i.e., the length of one arm of a half-wavelength dipole antenna), and σ_0 is the dc conductivity of bulk copper. It can be seen that a 50 nm radius MWCNT can provide approximately a factor of five improvement compared to copper, resulting in 1% radiation efficiency (which is not reached for a copper wire until $a = 100$ nm). The MWCNT curve is only shown till $a = 100$ nm, and, in fact, most tubes have $a \lesssim 50$ nm. Furthermore, if the tube circumference becomes too large, the loss of phase coherence around the perimeter of the tube may invalidate the derived formula.

The curves labeled MWCNT in Fig. 7 are similarly obtained, although in each case the nanotube length was adjusted to be a quarter wavelength at the various frequencies (the upper curve is for 10 GHz, the middle curve for 100 GHz, and the lower curve, 1 THz). It can be seen that in each case a significant improvement over copper can be obtained.

Finally, it should be mentioned that measurements on a parallel array of large-diameter MWCNTs showed free-space $\lambda/2$ resonant effects in the optical band [54], confirming the high conductivity of large radius MWCNTs even at optical frequencies. Therefore, currently, large-radius ($a \sim 50$ nm) MWCNTs seem to be good candidates for nano-radius antenna applications (even through optical frequencies). MWCNT antennas are also discussed in [55].

VII. Conclusions

The radiation efficiency of nano-radius wire antennas is very low due to large impedances and the associated high ohmic losses at these sizes. The surface impedance of nanoradius wires has been discussed, and the relationship between wire radius, frequency, conductivity, and ohmic loss has been illustrated for dipole antennas. The connection between the current on a wire antenna, and the current associated with the principle discrete propagation mode on an infinitely-long metallic wire has been discussed, both of which provide complementary ways to view the attenuation problems of nanoradius wires. Several possible methods to improve the radiation efficiency of sub-100 nm radius dipole antennas have been considered, including the use of superconductors and multi-wall carbon nanotubes.

Acknowledgements

The author would like to thank Azad Naeemi, Georgia Institute of Technology, for helpful comments.

References

[1] Stutzman, W.L. and G.A. Thiele, *Antenna Theory and Design*, 2nd Edition, John Wiley & Sons, New York, 1998.

[2] Burke, P.J., S. Li, and Z. Yu, "Quantitative theory of nanowire and nanotube antenna performance," *IEEE Trans. Nanotech.*, v. 5, pp. 314-334, July 2006.

[3] Podolskiy, V.A., A.K. Sarychev, E.E. Narimanov, and V.M. Shalaev, "Resonant light interaction with plasmonic nanowire systems," *J. Opt. A*, v.7, pp. S32-S37, 2005.

[4] Fromm, D.P., A. Sundaramurthy, P. J. Schuck, G. Kino, and W.E. Moerner, "Gap-dependent optical coupling of single "bowtie" nanoantennas resonant in the visible," *Nano Letters*, v. 4, no. 5, pp. 957-961, 2004.

[5] Schuck, P.J., D.P. Fromm, A. Sundaramurthy, G.S. Kino, and W.E. Moerner, "Improving the mismatch between light and nanoscale objects with gold bowtie nanoantennas," *Phys. Rev. Lett.*, v. 94, pp. 017402:1-4, 2005.

[6] Mühlschlegal, H.-J. Eisler, O.J.F. Martin, B. Hecht, and D.W. Pohl, "Resonant optical antennas," *Science*, v. 308, pp. 1607-1609, 2005.

[7] Alda, J., J.M. Rico-García, J.M. López, and G. Boreman, "Optical antennas for nano-photonic applications," *Nanotechnology*, v. 16, pp. S230-S234, 2005.

[8] Novotny, L., "Effective wavelength scaling for optical antenna," *Phys. Rev. Lett.*, v. 98, pp. 266802(1-4), 2007.

[9] Alù, A. and N. Engheta, "Input Impedance, Nanocircuit loading, and radiation tuning of optical nanoantennas," *http://arxiv.org/abs/0710.3411,* 2007.

[10] Aizpurua, J., G.W. Bryant, L.J. Richter, and F. J. García de Abajo, "Optical properties of coupled metallic nanorods for field-enhanced spectroscopy," *Phys. Rev. B.*, v. 71, pp. 235420(1-13), 2005.

[11] King, R.W.P., and T.T. Wu "The imperfectly conducting cylindrical transmitting antenna," *IEEE Trans. Antennas. Propagat.*, v. AP-14, pp. 524-534, Sept. 1966.

[12] Richmond, J.H. "Scattering by imperfectly conducting wires," *IEEE Trans. Antennas. Propagat.*, v. AP-15, pp. 802-806, Nov. 1967.

[13] Hanson, G.W., "On the Applicability of the Surface Impedance Integral Equation for Optical and Near Infrared Dipoles," *IEEE Trans. Antennas Propagat*., v. 54, pp. 3677-3685, Dec. 2006.

[14] Stratton, J.A. *Electromagnetic Theory*, McGraw-Hill: New York, 1941.

[15] Wu, T.T. "Introduction to linear antennas," in *Antenna Theory*, Ch. 8, Part 1, R.E. Collin and F.J. Zucker, Eds. McGraw-Hill: New York, 1969.

[16] Hallén, E. *Electromagnetic Theory*, John Wiley and Sons: New York, 1962.

[17] Hanson, G.W., "Fundamental Transmitting Properties of Carbon Nanotube Antennas," *IEEE Trans. Antennas. Propagat.*, v. 53, pp. 3426-3435, Nov. 2005

[18] Werner, D.H., J.A. Huffman, and P.L. Werner, "Techniques for evaluating the uniform current vector potential at the isolated singularity of the cylindrical wire kernel," *IEEE Trans. Antennas. Propagat.*, v. 42, pp. 1549-1553, Nov. 1994.

[19] Jones, D.S. *Methods in Electromagnetic Wave Propagation*, IEEE Press: New Jersey, 1994.

[20] Kittel, C., *Introduction to Solid State Physics*, 6^{th} Ed. Wiley: New York, 1986.

[21] Steinhögl, W., G. Schindler, G. Steinlesberger, M. Traving, and M. Engelhardt (2005). "Comprehensive study of the resistivity of copper wires with lateral dimensions of 100 nm and smaller," *J. Appl. Phys.,* v. 97, pp. 023706:1–7.

[22] Bid, A., A. Bora, and A. K. Raychaudhuri, "Temperature dependence of the resistance of metallic nanowires of diameter $\geq$ 15 nm: Applicability of Bloch-Grüneisen theorem," *Phys. Rev. B*., v. 74, pp. 035426: 1-8, 2006.

[23] Abramowitz, M. and I. A. Stegun, *Handbook of Mathematical Functions*, National Bureau of Standards, 1964.

[24] Van Duzer, T., and C.W. Turner, *Principles of Superconductive Devices and Circuits*, Elsevier: New York, 1981.

[25] Lide, D.R. (Editor), *CRC Handbook of Chemistry and Physics*, 87th Edition, CRC Press: Boca Raton, 2006.

[26] Zgirski, M., K-P Riikonen, V. Touboltsev, and K. Arutyunov, "Size Dependent Breakdown of Superconductivity in Ultranarrow Nanowires," *Nano Lett*., v. 5, pp. 1029-1033, 2005.

[27] Tian, M., J. Wang, J.S. Kurtz, Y. Liu, M.H W. Chan, T.S. Mayer, and T.E. Mallouk, " Dissipation in quasi-one-dimensional superconducting single-crystal Sn nanowires," *Phys. Rev. B*, v. 71, pp. 104521: 1-7, 2005.

[28] Tian, M., J. Wang, J. Snyder, J. Kurtz, Y. Liu, P. Schiffer, T.E. Mallouk, and M.H.W. Chen, "Synthesis and characterization of superconducting single-crystal Sn nanowires," *Appl. Phys. Letts.*, v. 83, pp. 1620-1622, 2003.

[29] Hansen, R.C., *Electrically Small, Superdirective, and Superconducting Antennas*, Wiley: New Jersey, 2006.

[30] Mansour, R.R., "Microwave superconductivity," *IEEE Trans. Microwave Theory Tech*., v. 50, pp. 750-759, Mar. 2002.

[31] Wuensch, S., G. Benz, E. Crocoll, M. Fitsilis, M. Neuhaus, T.A. Scherer, W. Jutzi, " Normal and superconductor coplanar waveguides with 100 nm linewidth," *IEEE Trans. Appl. Supercond.*, v. 11, pp. 115-118, Mar. 2001.

[32] Jutzi, W., S. Wuensch, E. Crocoll, M. Neuhaus, T.A. Scherer, T. Weimann, J. Niemeyer, "Microwave and DC properties of niobium coplanar waveguides with 50-nm linewidth on silicon substrates," *IEEE Trans. Appl. Supercond.*, v. 13, pp. 320-323, June 2003.

[33] R. Saito, G. Dresselhaus, and M.S. Dresselhaus, *Physical Properties of Carbon Nanotubes*, Imperial College Press: London, 2003.

[34] Ryu, C., K-W Kwon, A.L.S. Loke, H. Lee, T. Nogami, V.M. Dubin, R.A. Kavari, G.W. Ray, S.S. Wong, "Microstructure and Reliability of Copper Interconnects," *IEEE Trans. Electron Devices*, v. 46, pp. 1113-1120, June 1999.

[35] Molares, M.E.T., E. M. Höhberger, Ch. Schaeflein, R. H. Blick, R. Neumann, and C. Trautmann, "Electrical characterization of electrochemically grown single copper nanowires," *Appl. Phys. Letts*, v. 82, pp. 2139-2141, 2003.

[36] Hanson, G.H., "Current on an Infinitely-Long Carbon Nanotube Antenna Excited by a Gap Generator," *IEEE Trans. Antennas Propagat.*, v. 54, pp. 76-81, Jan. 2006.

[37] Slepyan, G. Ya., M.V. Shuba, S.A. Maksimenko, and A. Lakhtakia, "Theory of optical scattering by achiral carbon nanotubes and their potential as optical nanoantennas," *Phys. Rev. B*, v. 73, p. 195416: 1-11, 2006.

[38] Miano, G., and F. Villone, "An Integral Formulation for the Electrodynamics of Metallic Carbon Nanotubes Based on a Fluid Model," *IEEE Trans. Antennas Propagat.*, v. 54, pp. 2713-2724, Oct. 2006.

[39] Slepyan, G. Ya., S.A. Maksimenko, A. Lakhtakia, O. Yevtushenko, and A.V. Gusakov, "Electrodynamics of carbon nanotubes: Dynamic conductivity, impedance boundary conditions, and surface wave propagation," *Phys. Rev. B*, v. 60, pp. 17136-17149, Dec. 1999.

[40] Maksimenko, S.A., and G.Y. Slepyan, "Electrodynamic properties of carbon nanotubes," in O.N. Singh and A. Lakhtakia, Eds., *Electromagnetic Fields in Unconventional Materials and Structures*, Wiley: New York, 2000.

[41] Jishi, R.A., M.S. Dresselhaus, and G. Dresselhaus, "Electron-phonon coupling and the electrical conductivity of fullerene nanotubes," *Phys. Rev. B*, v. 48, pp. 11385-11389, 1993.

[42] Zhou, X., J-Y Park, S. Huang, J. Liu, and P.L. McEuen, " Band Structure, Phonon Scattering, and the Performance Limit of Single-Walled Carbon Nanotube Transistors," *Phys. Rev. Lett*. v. 95, pp. 146805:1-4, 2005.

[43] Burke, P.J., "Lüttinger liquid theory as a model of the GHz electrical properties of carbon nanotubes," *IEEE Trans. Nanotechnol.*, v. 1, pp. 129-144, Sept. 2002.

[44] Burke, P.J., "An RF circuit model for carbon nanotubes," *IEEE Trans. Nanotechnol.*, v. 2, pp. 55-58, March 2003.

[45] Salahuddin, S., M. Lundstrom, and S. Datta, "Transport Effects on Signal Propagation in Quantum Wires," *IEEE Trans. Electron Devices*, v. 52, pp. 1734-1742, Aug. 2005.

[46] Yu, Z., and P. J. Burke, "Microwave transport in metallic single-walled carbon nanotubes," *Nano Letters*, v. 5, pp. 1403-1406, 2005.

[47] Naeemi, A., and J.D. Meindl, "Impact of Electron-Phonon Scattering on the Performance of Carbon Nanotube Interconnects for GSI," *IEEE Electron Device Letts*., v. 26, pp. 476-478, July 2005.

[48] Naeemi, A., R. Sarvari, and J. D. Meindl, "Performance comparison between carbon nanotube and copper interconnects for gigascale integration (GSI)," *IEEE Electron Device Lett*., v. 26, pp. 84–86, Feb. 2005.

[49] Nieuwoudt, A., and Y. Massoud, "Evaluating the Impact of Resistance in Carbon Nanotube Bundles for VLSI Interconnect Using Diameter-Dependent Modeling Techniques," *IEEE Trans. Electron Devices*, v. 53, pp. 2460-2466, Oct. 2006.

[50] Massoud, Y., and A. Nieuwoudt, "Modeling and design challenges and solutions for carbon nanotube-based interconnect in future high performance integrated circuits,"*ACM Journal on Emerging Technologies in Computing Systems (JETC)*, v. 2, pp. 155-196, July 2006.

[51] Li, H.J., W.G. Lu, J.J. Li, X.D. Bai, and C. Z. Gu, "Multichannel Ballistic Transport in Multiwall Carbon Nanotubes," *Phys. Rev. Letts*., v. 95, pp. 086601:1-4, 2005.

[52] Naeemi, A., and J.D. Meindl, "Compact Physical Models for Multiwall Carbon-Nanotube Interconnects," *IEEE Electron Device Letts*., v. 27, pp. 338-340, May 2006.

[53] Wei, B.Q., R. Vajtai, and P. M. Ajayan, "Reliability and current carrying capacity of carbon nanotubes," *Appl. Phys. Letts.*, v. 79, pp. 1172-1174, 2001.

[54] Wang, Y., K. Kempa, B. Kimball, J.B. Carlson, G. Benham, W.Z. Li, T. Kempa, A. Rybczynski, and Z.F. Ren, "Receiving and transmitting light-like radio waves: Antenna effect in arrays of aligned carbon nanotubes," *Applied Physics Letters*, v. 85, pp. 2607-2609, Sept. 2004.

[55] Lan, Y., and B. Zeng, "Properties of Carbon Nanotube Antenna," International Conference on Microwave and Millimeter Wave Technology (ICMMT), April 2007.